International Journal of Architectural, Civil and Construction Sciences
ISSN: 2415-1734
Vol:6, No:10, 2012

Geometric and Material Nonlinear Analysis of Reinforced Concrete Structure Considering Soil-Structure Interaction

Mohamed M. El-Gendy, Ibrahim A. El-Arabi, Rafik W. Abdel-Missih, Omar A. Kandil

***Abstract*—**In the present research, a *finite element model* is presented to study the geometrical and material nonlinear behavior of reinforced concrete plane frames considering soil-structure interaction. The nonlinear behaviors of concrete and reinforcing steel are considered both in compression and tension up to failure. The model takes account also for the number, diameter, and distribution of rebar along every cross section. Soil behavior is taken into consideration using four different models; namely: *linear-*, *nonlinear Winkler's model*, and *linear-*, *nonlinear continuum model*. A computer program (NARC) is specially developed in order to perform the analysis. The results achieved by the present model show good agreement with both theoretical and experimental published literature. The nonlinear behavior of a rectangular frame resting on soft soil up to failure using the proposed model is introduced for demonstration.

***Keywords*—**Nonlinear analysis, Geometric nonlinearity, Material nonlinearity, Reinforced concrete, Finite element method, Soil-structure interaction, Winkler's soil model, Continuum soil model

I. Introduction

GEOMETRICAL and material nonlinear analysis is considered one of the most important design and safety tools in structural engineering. In the classical analysis methods of plane framed structures, the axial and flexural rigidities are assumed to be constants, and the supports are considered to be perfect. However, such ideal conditions are unrealistic because the material behavior is actually nonlinear and perfect supports do not exist in reality. The axial and flexural rigidities certainly decrease with the increasing internal forces. The structure geometry is continuously changing with the varying applied forces too. Moreover, the column footings are mostly resting on deformable soil. Therefore, developing a step-by-step nonlinear analysis method to investigate such real situations up to failure is essential.

Many authors studied the monotonic behavior of reinforced concrete structures having different cross-sectional shapes and subjected to biaxial bending and axial forces. Dunder [1] studied the monotonic behavior of reinforced concrete members with perfect supports; assuming a symmetric distribution of steel reinforcement over the rectangular cross section.

M. M. El-Gendy, Professor of Foundation Eng., Faculty of Engineering, Port Said University, Port Said, Egypt (e-mail: MElgendy@elpla.com).
I. A. El-Arabi, Associate Professor, Faculty of Engineering, Port Said University, Port Said, Egypt (e-mail: iielarabiii@yahoo.com).
Rafik W. Abdel-Missih, Assistant Professor, Faculty of Engineering, Port Said University, Port Said, Egypt (e-mail: Dr_RafeekWS@hotmail.com).
Omar A. Kandil, Ph. D. Candidate, Faculty of Engineering, Port Said University, Egypt (e-mail: OmarKandil@hotmail.com).

Kwat and Filippou [2] studied the nonlinear characteristics of reinforced concrete structures provided with perfect supports under monotonic loads.

Concrete and reinforcing steel bars were represented by separate material models. Anam and Shoma [3] and Ibrahim and Zubydan [4] studied the structural behavior of perfectly supported reinforced concrete frames taking both the geometrical and material nonlinear effect into account.

Other authors studied the structural behavior of frames considering soil structure interaction. Hassan [5] studied the elastic stability of uncracked and cracked plane frames resting on elastic soil. Based on a nonlinear material model, Jahromi *et-al* [6] studied the soil structure interaction of steel frames with elastic reinforced concrete footings resting on elastic soil.

In this research a new *finite element model* is presented to analyze the nonlinear behavior of plane reinforced concrete frames. Variations of axial and flexural rigidities along the frame members are investigated. The effects of material and geometrical nonlinearity are considered. Moreover, the soil-structure interaction is considered via four different soil models. The proposed model is able to predict the normal stress distribution over the cross-section, straining actions, crack depth, residual rigidities along the members, structure deformed shape, and the settlement. Real stress-strain curves of concrete and reinforcing steel are considered in the analysis.

II. Finite Element Model of Reinforced Concrete Superstructures

A. Material modeling

The nonlinear stress-strain behaviors of concrete and reinforcing steel were investigated earlier by many researchers [2, 3, 4, 7, 8, and 9]. The material models adopted in the present work, are discussed in this section.

1. Concrete in compression

Fig. 1 shows the stress-strain relationship of concrete in compression as given by Ibrahim and Zubydan [4]. For unconfined sections (without stirrups), the relation is modeled by a parabolic curve up to the maximum strength (σ_{co}) followed by a descending linear response till failure. For confined sections (with stirrups), a similar model is considered as shown in the figure. It should be noticed that the crushing strain of a confined section (ε_m) is much higher than that of an unconfined section (ε_{uc}).

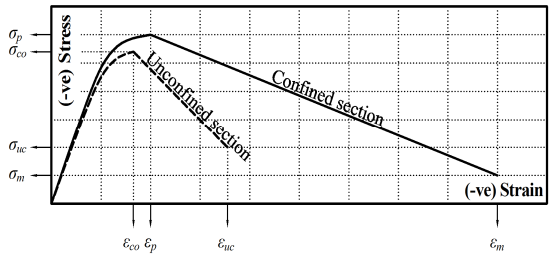

Fig. 1 Stress-strain relationship of concrete in compression

2. Concrete in tension

The stress-strain relationship of concrete in tension is illustrated in Fig. 2, [8 and 9]. It can be clearly observed that the tensile strength of concrete increases linearly with increasing strain up to cracking. At cracking strain (ε_{cr}), a small subsequent drop in tensile strength occurs. The tensile strength then decreases monotonically with increasing strain up to failure.

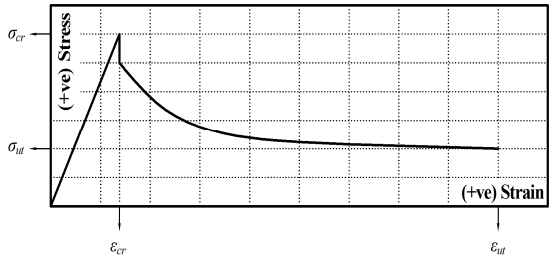

Fig. 2 Stress-strain relationship of concrete in tension

3. Reinforcing steel

Fig. 3 shows a typical stress-strain relationship of steel in tension and compression. The behavior is almost linear-elastic up to the yield strength. The strain increases up to the hardening point without increasing in stress. After that, the stress increases again with strain forming a strain-hardening region up to the ultimate strength, [4 and 8].

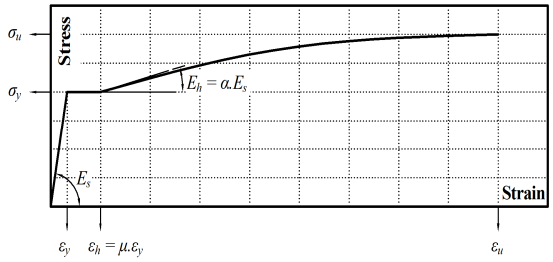

Fig. 3 Stress-strain relationship of reinforcing steel

4. Analysis of reinforced concrete sections

The proposed nonlinear model of reinforced concrete sections subjected to axial force and bending is developed in this section.

The following assumptions are adopted in order to simplify the analysis:

- Strain distribution is assumed to be linear along the section while the stress distribution is nonlinear.
- The bond between concrete and reinforcing steel is assumed to be perfect.
- Deformations due to shear and torsion are neglected.

The forces acting on a reinforced concrete section are resisted by the stresses both in concrete and reinforcement. Fig. 4 shows a reinforced concrete section subjected to an axial force (N) and a bending moment (M) with the corresponding strain and stress distributions. For any cross-section, the longitudinal normal stresses in both the concrete and reinforcing steel should be in equilibrium with the stresses due to N and M. Therefore, the following two conditions of equilibrium must be satisfied:

$$\Sigma F_c + \Sigma F_s = N \tag{1}$$

$$\Sigma M_c + \Sigma M_s = M + N.e_n \tag{2}$$

Where,

ΣF_c, ΣF_s = summation of forces due to stress distribution in concrete and steel, respectively,

ΣM_c, ΣM_s = summation of moments due to stress distribution in concrete and steel, respectively,

e_n = Location of neutral axis measured from centroidal axis.

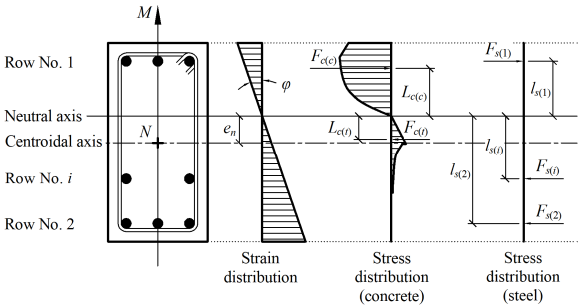

Fig. 4 Strain and stress distributions on a reinforced concrete section subjected to axial force and bending moment

The solution of this couple of nonlinear equations should be carried out using a *finite element technique*. In this case, the cross-section is divided into a number of equal concrete strips as shown in Fig 5. The strains for each strip are functions of the cross section curvature (φ) and the neutral axis location (e_n), while the stresses, in turn, are functions of the strains. The normal stress distribution on each concrete strip is numerically integrated in order to obtain the force and moment acting on that strip. The sum the forces (and moments) for all strips and rebar gives the total reinforced concrete section normal force (and moment), respectively.

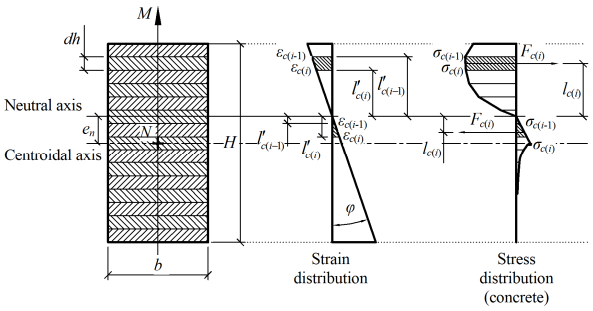

Fig. 5 *Finite element technique* for concrete section

It is clear that the problem is basically dependent on two related unknowns; namely: the neutral axis position (e_n), and the curvature of cross-section (φ). Therefore, the problem is solved iteratively using the *modified Newton-Raphson iteration method* [10].

B. Force-displacement relationship

If a structure is in the state of stable equilibrium and the small displacement theory is valid, then there is a relationship between the deformations of the structure and the applied load system. For the plane frame element shown in Fig. 6, the load-displacement relationship can be expressed by:

$$[k_T]_i \times \{d\delta\}_i = \{dF\}_i \tag{3}$$

Where,
$[k_T]_i$ = tangential stiffness matrix for the i^{th} element,
$\{d_\delta\}_i$ = displacements vector for the i^{th} element,
$\{d_F\}_i$ = force vector for the i^{th} element,

The tangential stiffness matrix $[k_T]$ is composed of two components and can be written as:

$$[k_T]_i = [k_m]_i + [k_g]_i \tag{4}$$

Where,
$[k_m]_i$ and $[k_g]_i$ = material and geometrical stiffness matrix for the i^{th} element, respectively,

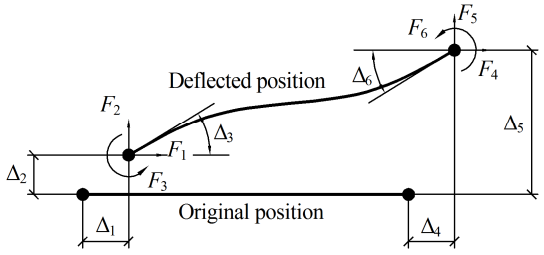

Fig. 6 End forces and displacements of a plane frame element

The geometric stiffness matrix $[k_G]$ for frame element is given by:

$$[k_g] = \frac{\pm P}{L}\begin{bmatrix} 0 & 0 & 0 & 0 & 0 & 0 \\ 0 & \frac{6}{5} & \frac{L}{10} & 0 & -\frac{6}{5} & \frac{L}{10} \\ 0 & \frac{L}{10} & \frac{2L^2}{15} & 0 & -\frac{L}{10} & -\frac{L^2}{30} \\ 0 & 0 & 0 & 0 & 0 & 0 \\ 0 & -\frac{6}{5} & -\frac{L}{10} & 0 & \frac{6}{5} & -\frac{L}{10} \\ 0 & \frac{L}{10} & -\frac{L^2}{30} & 0 & -\frac{L}{10} & \frac{2L^2}{15} \end{bmatrix} \tag{5}$$

Where,
$\pm P$ = tensile or compressive axial force,
L = length of frame element.

It is clearly observed that the geometrical stiffness matrix $[k_g]$ depends on the axial force P. It expresses the decrease in the flexure stiffness due to the presence of a compressive axial force. The negative sign corresponds to a compressive axial force, and vice versa.

Equation (3) is formed in an incremental form since the use of the geometric matrix to capture the second-order effects requires a stepwise application of the applied loads. This matrix should be updated, at every load step, based on the resulting axial forces in the frame elements, [4, 11, and 12].

III. Soil Modeling

In fact, the soil layers move down under vertical compressive loading. In this work, 4 different soil models are considered to investigate the soil-structure interaction. These models are *linear-*, *nonlinear Winkler's soil models*, and *linear-*, *nonlinear continuum soil models*.

A. Linear Winkler's soil model

This model assumes that the soil model is represented by an infinite number of elastic springs. The settlement ($S_{(i)}$) of the soil at any point (i) on the surface is directly proportional to the soil pressure at this point ($q_{(i)}$) as shown in Fig. 7. For an element at the i^{th} location the contact pressure is given by:

$$q_{(i)} = K_{s(i)} \times S_{(i)} \tag{6}$$

Where,
$K_{s(i)}$= modulus of subgrade reaction at point i.

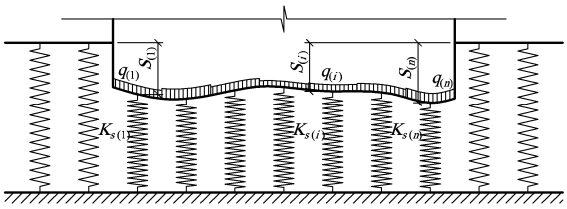

Fig. 7 Surface displacement of the *Winkler's model*

B. Nonlinear Winkler's model

In the previous model the contact pressure-settlement relationship is linear as shown in Fig. 8. In fact, this relationship is nonlinear. Referring to Fig. 7, the nonlinear contact pressure ($q_{n(i)}$) at the i^{th} location is given by the following hyperbolic function:

$$q_{n(i)} = \frac{S_{(i)}}{\frac{1}{K_{s(i)}} + \frac{S_{(i)}}{q_u}} \tag{7}$$

Where,

q_u= geometrical parameters.

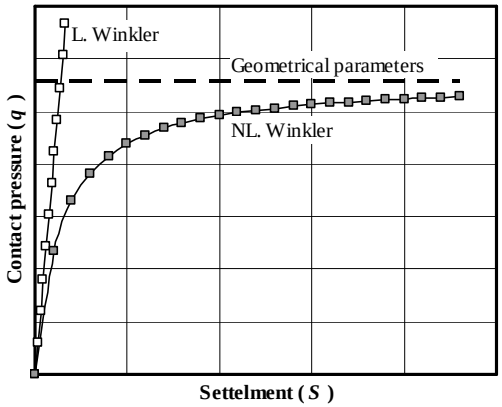

Fig. 8 Contact pressure-settlement relationship for *linear* and *nonlinear Winkler's model*

C. Continuum soil model

In fact, the surface settlement of soil media that possess a slight amount of cohesion will occur not only under loaded region, but also within certain limited zones outside the loaded region as shown in Fig. 9. This phenomenon restricts the applicability of *Winkler's model*. In order to account for this continuous behavior, soil media is often idealized as *continuum model*. Analysis of foundation using *continuum soil model* requires obtaining the *modules of elasticity* of the soil (E_s), [13].

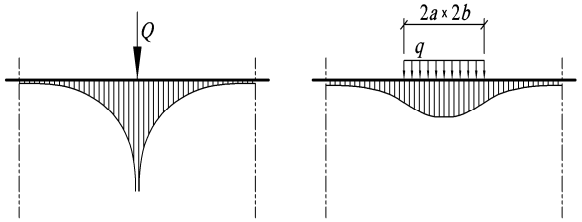

(a) A concentrated load (Q). (b) A uniform load (q) of area ($2a \times 2b$).

Fig. 9 Typical stress distribution of soil for *continuum model*

Referring to Fig. 10, the vertical stress ($\sigma_{z(i)}$) and settlement ($S_{(i)}$) at the i^{th} location in a specific layer due to a concentrated load (Q) is given by:

$$\sigma_{z(i)} = \frac{3QZ_{(i)}^3}{2\pi R^5} \tag{8}$$

$$S_{(i)} = \frac{1}{E_{s(i)}} \times \frac{3QZ_{(i)}^3}{2\pi R_{(i)}^3} \times H_{(i)} \tag{9}$$

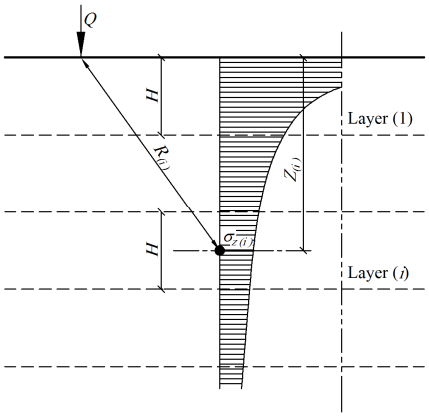

Fig. 10 Vertical stress distribution due to concentrated load using *continuum model*

For uniform load (q) of area ($2a \times 2b$) as shown in Fig. 11, the vertical stress ($\sigma^{\bullet}_{z(i)}$) due to quarter of load area under the corner of load ($a \times b$) is given by:

$$\sigma^{\bullet}_{z(i)} = \frac{q}{2\pi}\left[\left(\frac{1}{R_{1(i)}^2} + \frac{1}{R_{2(i)}^2}\right)\frac{a.b.Z_{(i)}}{R_{3(i)}} + \tan^{-1}\left(\frac{a.b}{Z_{(i)}.R_{3(i)}}\right)\right] \tag{10}$$

Where,

$$R_{1(i)} = \sqrt{a^2 + Z_{(i)}^2}$$

$$R_{2(i)} = \sqrt{b^2 + Z_{(i)}^2}$$

$$R_{3(i)} = \sqrt{a^2 + b^2 + Z_{(i)}^2}$$

Therefore, the vertical stress ($\sigma_{z(i)}$) and settlement ($S_{(i)}$) due to a uniform load (q) of area ($2a \times 2b$) under the center of load is given by:

$$\sigma_{z(i)} = 4 \times \sigma^{\bullet}_{z(i)} \tag{11}$$

$$S_{(i)} = \frac{H_{(i)}}{E_s} \times \sigma_{z(i)} \tag{12}$$

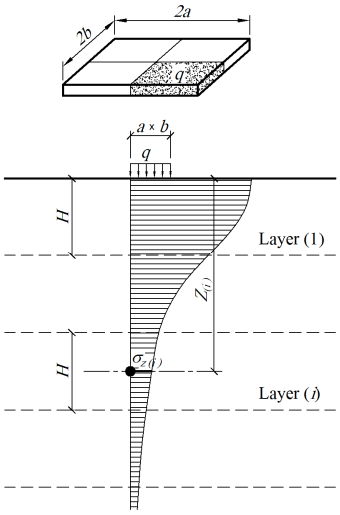

Fig. 11 Vertical stress distribution due to uniform load using *continuum* model

D.Relationship between Winkler's and continuum soil models

Equation (13) gives the relation between *modulus of subgrade reaction* (K_s) and *modules of elasticity* of the soil (E_s), [14].

$$K_s = \frac{E_s}{B \times I} \tag{13}$$

Where,

B= minimum dimension of foundation (m),

I= effect coefficient depend on (*d*/*B*, *L*/*B*) ratios [according to Fig. 12],

d= depth of foundation layers exposed to compression (m),

L= maximum dimension of foundation (m).

IV. Verification of The Model

A computer program called NARC (**N**onlinear **A**nalysis of **R**einforced **C**oncrete structures) is especially developed in order to carry out the analysis and to achieve the research goals. The program involves all above-mentioned constitutive models, formulations, and solution procedures. Structural failure of frames is assumed to occur when the stress in rebar reaches the ultimate limit. The program is capable to predict and plot the normal stress distribution along any cross-section, internal forces, deformed shapes (displacements), soil settlement, and axial- and flexural rigidity distributions on all members of the frame. The results of the proposed model are verified against theoretical and experimental data acquired from literature. Moreover, several study cases of R.C. structures subjected to general loading were analyzed nonlinearly up till collapse for demonstration.

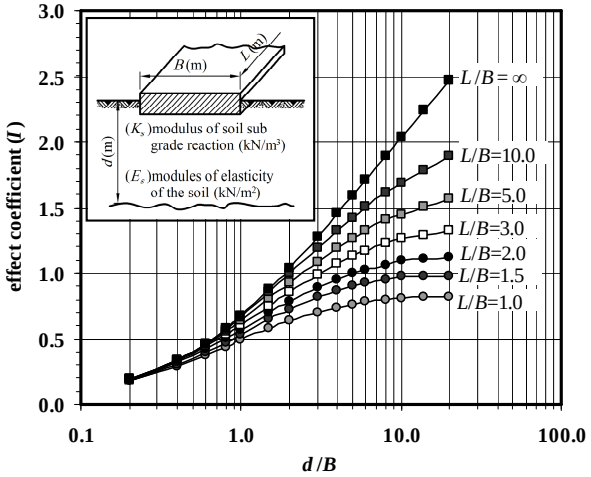

Fig. 12 Effect coefficient (*I*) versus (*d*/*B* & *L*/*B*), [14]

A. Comparison with experimental and theoretical beam test

The RC beam (VC3) detailed in Fig. 13 was tested earlier, experimentally by Juvandes [15], and theoretically by Stramandinoli and Rovere [9]. The beam is subjected to a twin concentrated loads as indicated. The predicted load-deflection response achieved by present model (NARC) is compared in Fig. 14, with the previously published experimental and theoretical results. A fairly good agreement is can be noticed, from the first loading stage up till 90% of the ultimate load. Theoretical predictions of NARC were accurate within 7% for the ultimate load, and within 9% for the maximum deflection just before failure.

B. Single-bay two-story frame test

Fig. 15 shows a full-scale single-bay two-story frame, which was tested by Vecchio and Emara [16]. The frame was designed with a span of 3.5m and a story height of 2.0 m. The frame was built integrally with a large and heavy reinforced concrete base.

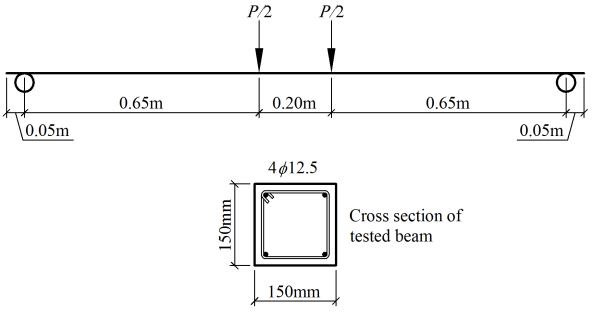

Fig. 13 Details of tested beam (VC3) tested by Juvandes [15]

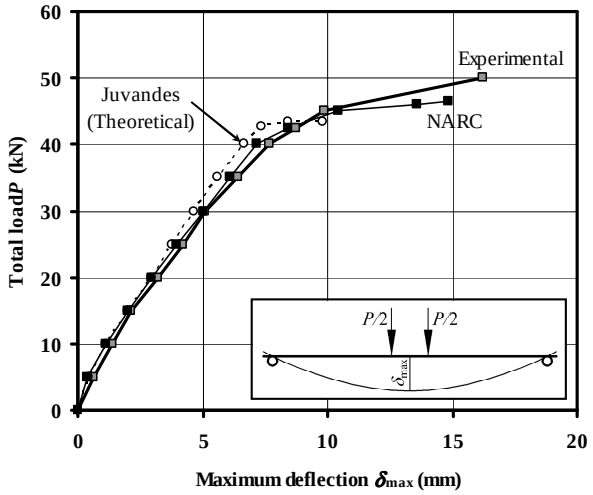

Fig. 14 Comparison between numerical and experimental results for VC3 beam tested by Juvandes [15]

All members of the frame were similarly reinforced with four (ϕ19.5mm) deformed bars as top and bottom reinforcement, and ϕ11.3mm closed stirrups at 125mm spacing as shear reinforcement. Placement of the reinforcement was such as to provide a clear cover of 30mm for the girders, and 20mm for the columns. Sections details and structure dimensions are also given in Fig. 15.

The concrete had a compressive strength (σ_{co}) of 30MPa. The ϕ19.5mm reinforcing steel bars, used as longitudinal reinforcement in all members were found to have a yield strength of 418MPa, an ultimate strength of 596MPa, a modulus of elasticity of 192,500MPa, and a strain-hardening modulus of 3,100MPa. For ϕ11.3mm bars used for shear reinforcement, the material properties had a yield strength of 454MPa and an ultimate strength of 640MPa. The frame was tested by applying a total axial load of 700kN to each column. Then, lateral load was applied monotonically until the ultimate capacity of the frame was achieved.

Fig. 16 shows comparisons between the predicted load-deflection responses for the first and top stories using (NARC) and the experimental results, [16]. It can be clearly observed that the analytical and experimental results are generally in a good agreement from the start up till 85% of the experimental ultimate load. The NARC prediction for ultimate load was found to be 15% higher, while the corresponding NARC deflections found to agree with the measured experimental deflections within 5% difference. This means that the proposed model NARC could reasonably predict the actual response of the test frame with acceptable discrepancy.

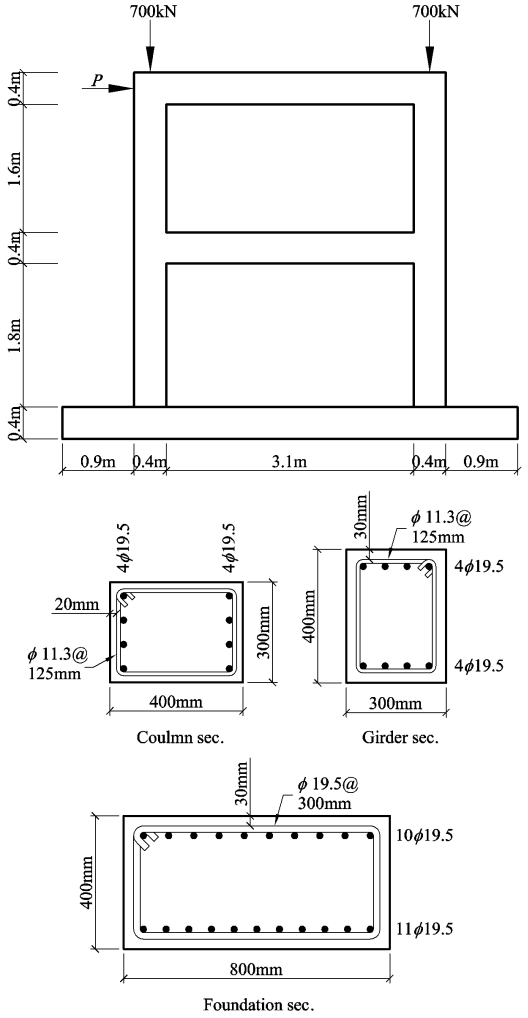

Fig. 15 Details of test single-bay two-story frame tested by Vecchio and Emara [16]

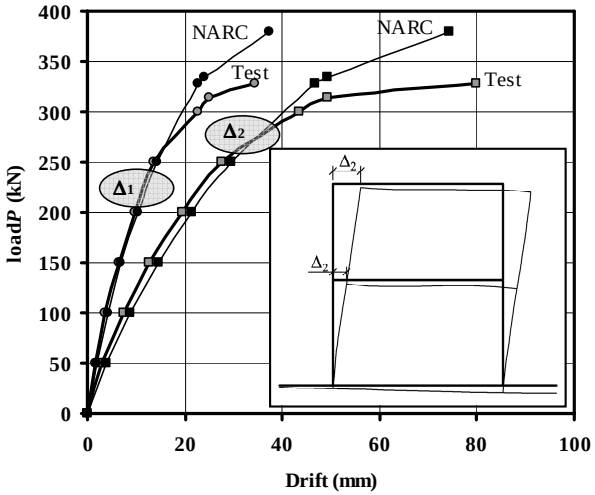

Fig. 16 A comparison between experimental results [16] and NARC results for a single-bay two-story frame

V. Nonlinear Analysis of Framed Structures Considering Soil-Structure Interaction

The efficiency of the developed computer code (NARC) for geometrical and material nonlinear analysis of RC frames considering soil-structure interaction, is studied in this section. The study case is given in Fig. 17. The shown 8m-wide, 4m-high rectangular frame was designed according to (ECCS 203-2001) code. The frame is founded by a 10m-long, 1m-wide strip footing. Details of cross sections and material properties for concrete and rebar are shown also in Fig. 17. The study case was analyzed several times assuming perfect support conditions at column bases, and by assuming real soil conditions under the footings too. 4-different soil models were considered; namely: *linear-*, *nonlinear Winkler's model*, and *linear-*, *nonlinear continuum model*. Table I lists the material parameters used in the analysis for both clay and sand soils. All study cases are summarized in Table II.

TABLE I
Relationship between Winkler's and continuum models

Soil profile	Clay soil	Sand soil
E_s (kN/m^2)	5000.0	50000.0
B (m)	1.0	1.0
d (m)	20.0	20.0
L (m)	10.0	10.0
I	1.8926	1.8926
K_s (kN/m^3)	2641.9	26418.7

TABLE II
Study cases for frames (supports and soil conditions)

Perfect support	Soil support	
	Clay soil	Sand soil
1. Hinged support	3. *L. Winkler's model* (K_s= 2641.9kN/m^3).	4. *L. Winkler's model* (K_s= 26418.7kN/m^3).
2. Fixed support	5. *NL. Winkler's model* (K_s= 2641.9kN/m^3).	6. *NL. Winkler's model* (K_s= 26418.7kN/m^3).
	7. *L. Continuum model* (E_s= 5000kN/m^2).	8. *L. Continuum model* (E_s= 50000N/m^2).
	9. *NL. Continuum model* (E_s= 5000kN/m^2).	10. *NL. Continuum model* (E_s= 50000N/m^2).

For the finite element discretization, all structural elements (the columns, girder, and foundation) were discretized into equal elements 0.5 m each. Externally applied load (w) was gradually increased up till failure (structural mechanism). Figure 18 shows the deformed shape of the frame at the ultimate load (w_u) as plotted by NARC for the 10-different analysis cases listed in Table II.

Figure 19 shows a histogram that describes the effect of base conditions on the ultimate capacity of RC frames. It can easily be noticed that the frame ultimate capacity is sensitive to soil type as well as the soil model; on which the analysis is based. Ultimate capacities of frames resting on clay are relatively lower, if compared with frames resting on sandy soils. Moreover, linear soil models give higher predictions for the ultimate loads, when compared with nonlinear models. All NARC results for soil-structure interaction models are bounded by the two idealized (hinged and fixed) solutions.

Figure 20 depicts a snap shot of the graphical output of NARC for the distribution of normal stresses and strains along a RC section.

The given plot shows the stress distribution on RC section located at the upper end of the right column for study case No. 4 (sand soil with *L. Winkler* model) at load (w = 122kN/m) just before the formation of plastic hinge. It is clear that the maximum compressive stress in concrete reached 40.8MPa while the tensile stress in rebar was 555.2MPa. The crack depth in this case was about 70% of the total depth of RC section. These results indicate that the considered RC section reached its ultimate capacity.

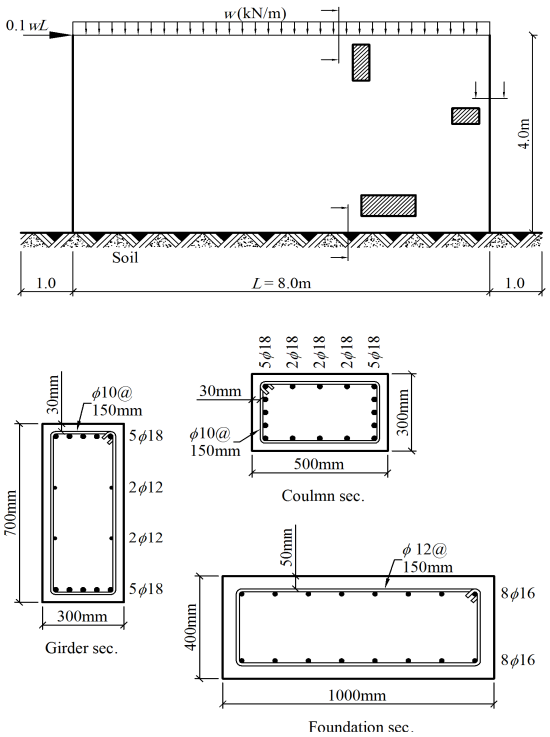

Fig. 17 Dimensions and details of rectangular frame

Section properties

Stirrup

- ϕ_{st} = 10mm (for column & girder).
- ϕ_{st} = 12mm (for foundation).
- No. of branches = 2.
- Stirrup spacing = 150mm.
- Yield strength = 360MPa.

Reinforced steel

- Yield strength = 400MPa.
- Ultimate strength = 600MPa.
- Young's modulus = 200,000MPa.
- Ultimate strain = 0.04.

Concrete

- Max. compressive strength = 40MPa.
- Max. tensile strength = 3.35MPa.

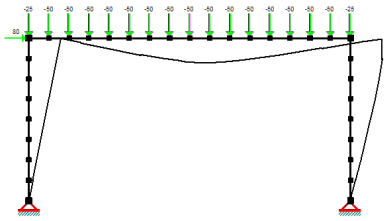

1. Hinged support (w_u= 100kN/m)
(Beam mechanism-Girder)

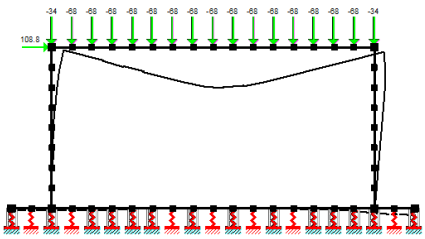

6. Sand (NL. Winkler) (w_u= 136kN/m)
(Combined mechanism)

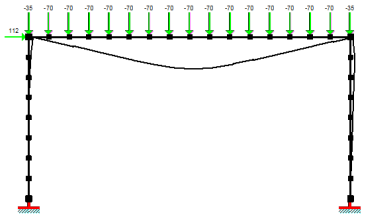

2. Fixed support (w_u= 140kN/m)
(Beam mechanism-Girder)

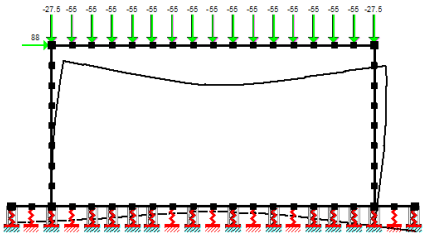

7. Clay (L. continuum) (w_u= 120kN/m)
(Beam mechanism-Foundation)

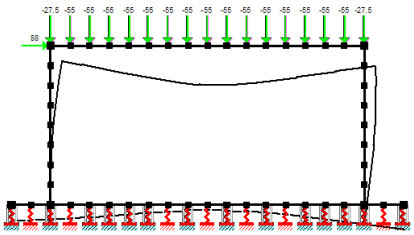

3. Clay (L. Winkler) (w_u= 110kN/m)
(Beam mechanism-Foundation)

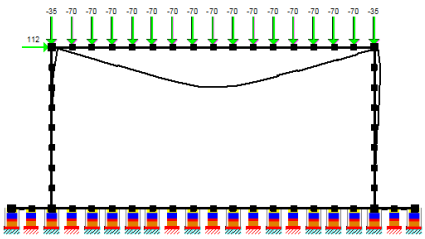

8. Sand (L. continuum) (w_u= 140kN/m)
(Beam mechanism-Girder)

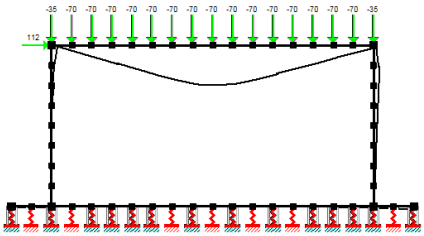

4. Sand (L. Winkler) (w_u= 140kN/m)
(Beam mechanism-Girder)

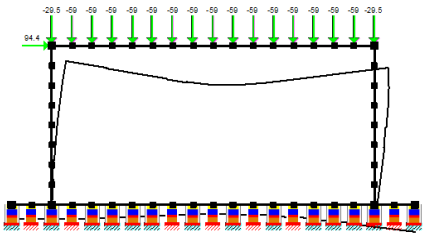

9. Clay (NL. continuum) (w_u= 118kN/m)
(Beam mechanism-Foundation)

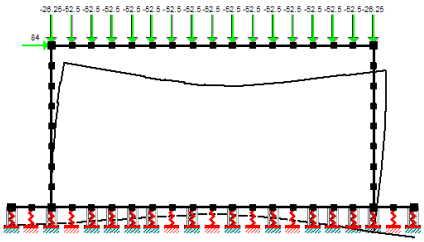

5. Clay (NL. Winkler) (w_u= 105kN/m)
(Beam mechanism-Foundation)

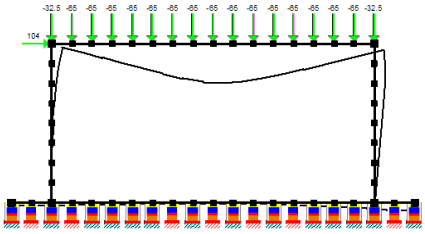

10. Sand (NL. continuum) (w_u= 130kN/m)
(Beam mechanism-Girder)

Fig. 18 Deformed shape of the frame at ultimate load (w_u) for 10-study cases listed in table II

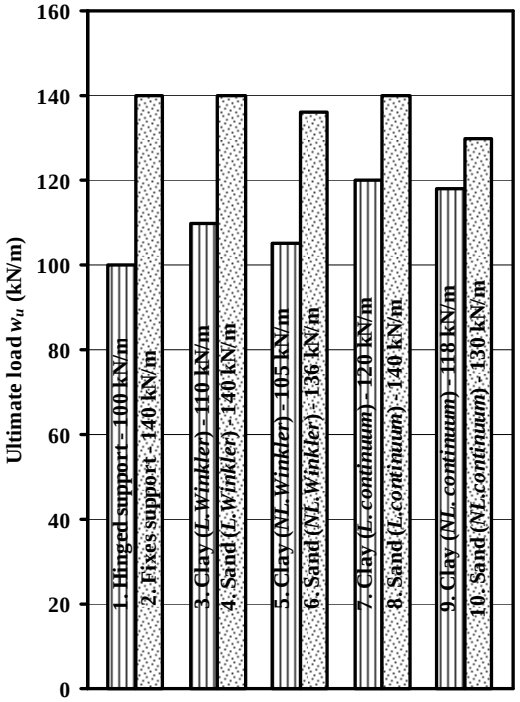

Fig. 19 Ultimate load (w_u) for different cases of soil model

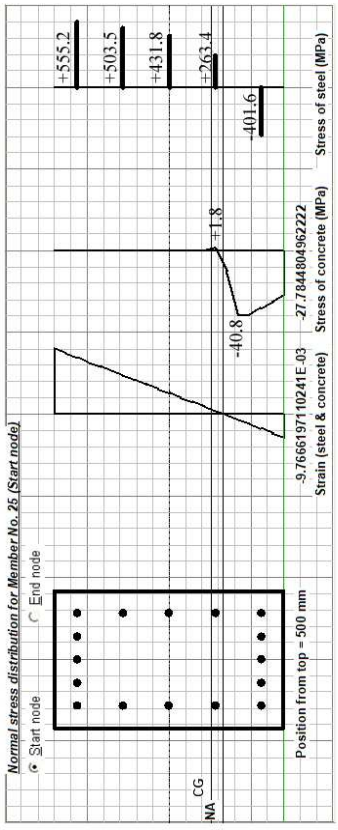

Fig. 20 Normal stress distribution on the cross section located at the upper end of the right column for study case No. 4 (sand soil with *L. Winkler* model) at load w = 122kN/m

Figures 21 through 24 show the comparisons between load-deflection curves obtained throughout soil structure interaction analyses carried out by NARC for the 4-soil models proposed in this work. In these figures, the abscissa shows the increase of frame drift at the left corner [mm], whereas the coordinate shows the increase in applied vertical load [kN/m]. The linear and nonlinear soil structure interaction response curves for every soil model are plotted, together with the response curves for the idealized hinged-hinged and fixed-fixed frames, for the sake of comparison. It is clear that the drift increases linearly with increasing loads up till cracking of the RC section located at the upper end of the right column. For further loading, the frame exhibits nonlinear strain hardening response up till the ultimate load level, which is encountered when the rebar fails at the same section. The results show that the response of frames resting on clayey soils is closer to that of a hinged-hinged frame. On the other hand, the behavior of frames founded by sandy soils is closer to that of a fixed-fixed frame. Predictions of the drift are generally higher for nonlinear soil models, except for sandy soils modeled by continuum model. For frames resting on clayey soils, the ultimate load predictions obtained by the continuum model are about 10% higher, if compared with Winkler's model predictions. However, the ultimate load predictions for frames resting on sandy soils are slightly sensitive the type of soil model considered in the analysis.

Variations of the bending moments at midspan of strip footing (M_1) and at the right column-base (M_3) with the applied load (w) are shown in Figs. 25 and 26. The abscissa in these figures shows the changes in bending moments [kNm], and the coordinate shows the increase in applied vertical load [kN/m]. Every figure shows 4-distinct curves for sand following the 4-considered soil models, besides 4-additional curves for clay. It is obvious from Fig. 25 that the bending moments (M_1) at midspan of strip footing are much greater for clay if compared with sand, at the same load level. However, the situation is different for the moment (M_3) at the right column-base as shown in Fig. 26. In this latter case, bending moments are smaller for clay if compared with sand, at the same load level. Figure 25 also shows that, the nonlinear results for bending moment (M_1) at midspan are bigger than the linear results, when the same category of soil model is considered. Moreover, bending moments (M_1) resulting from Winker's models are higher than those of the continuum model at the same load level.

These results of bending moments can be understood in context with the settlement behavior the frame as shown in Figs. 27 and 28. In these figures, the variations of settlements at midspan of strip footing (δ_1) and at the right column-base (δ_3) with the applied load (w) are shown. It should be emphasized here that the abscissa in Figs. 27 and 28 shows the increase in applied vertical load [kN/m], whereas the coordinate shows the settlement [mm]. Every figure shows 4-separate settlement curves for sand gathered from the 4-different soil models, besides 4-additional curves for clay. It is clear from these figures that the settlement is much bigger for clay if compared with sand, at the same load level.

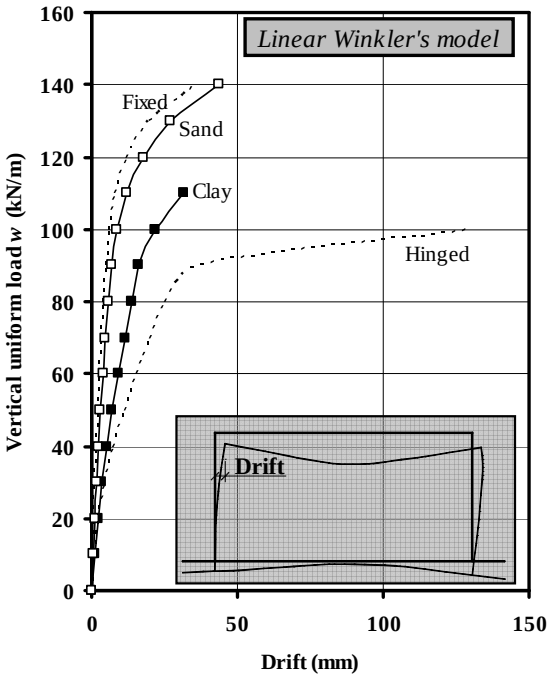

Fig. 21 Load versus drift for *linear Winkler's model*

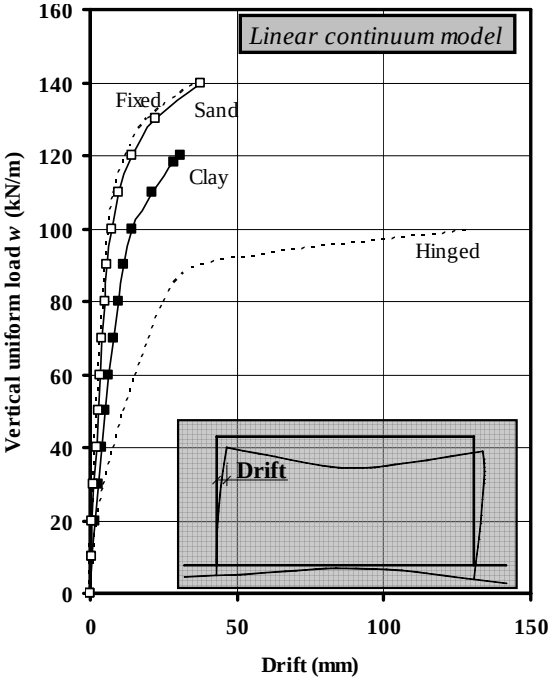

Fig. 23 Load versus drift for *linear continuum model*

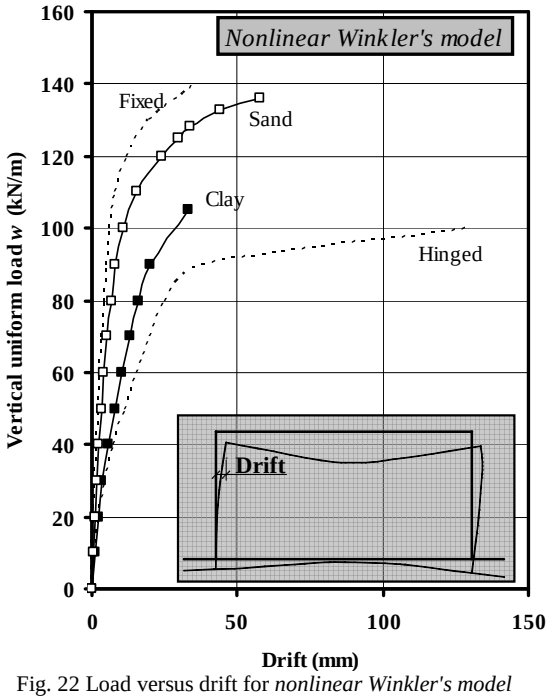

Fig. 22 Load versus drift for *nonlinear Winkler's model*

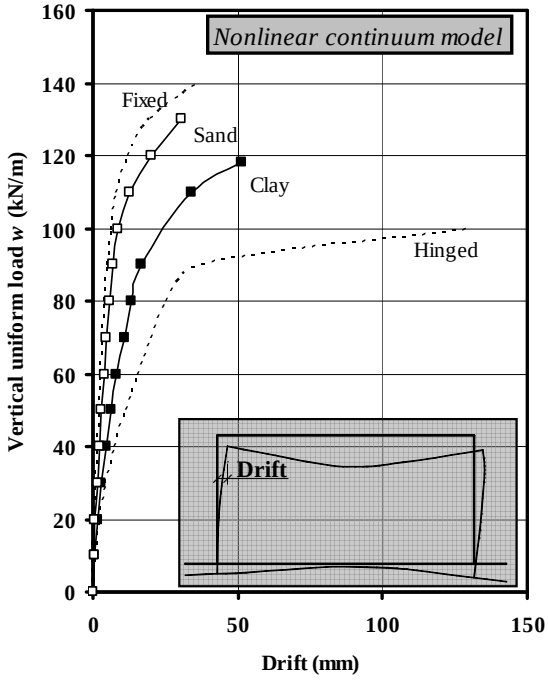

Fig. 24 Load versus drift for *nonlinear continuum model*

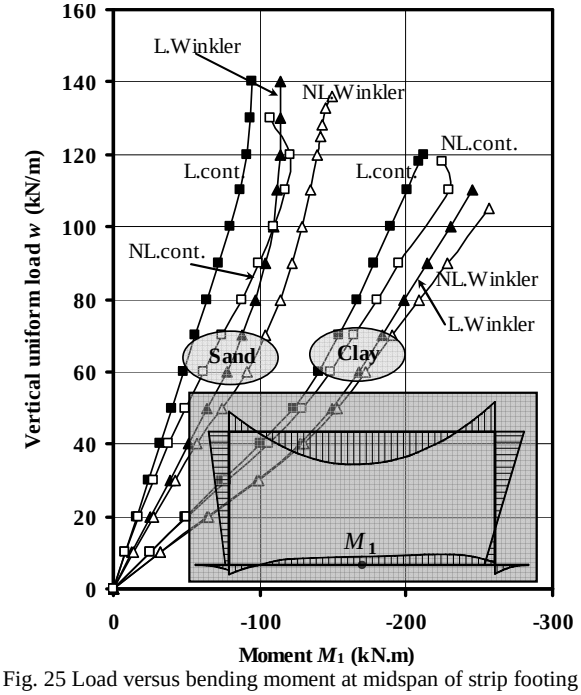

Fig. 25 Load versus bending moment at midspan of strip footing

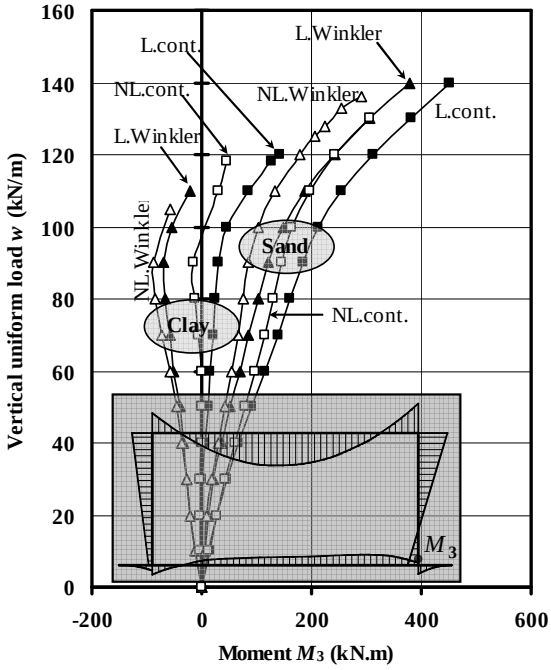

Fig. 26 Load versus bending moment at bottom section of right column.

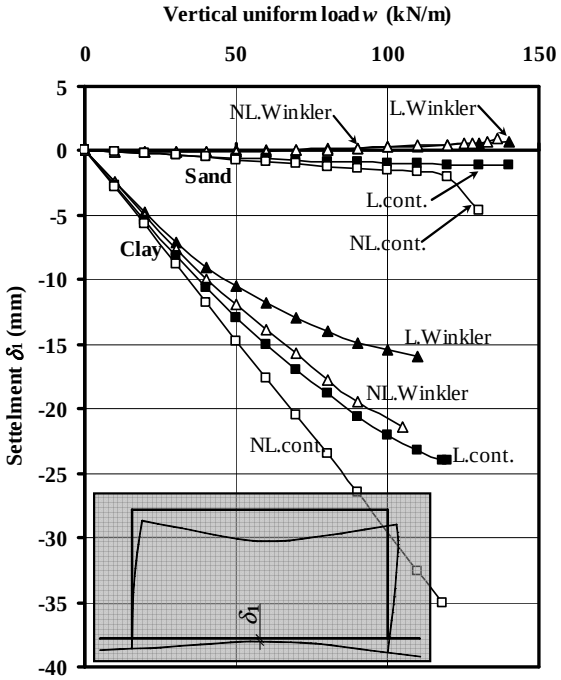

Fig. 27 Load versus settlement at midspan of strip footing

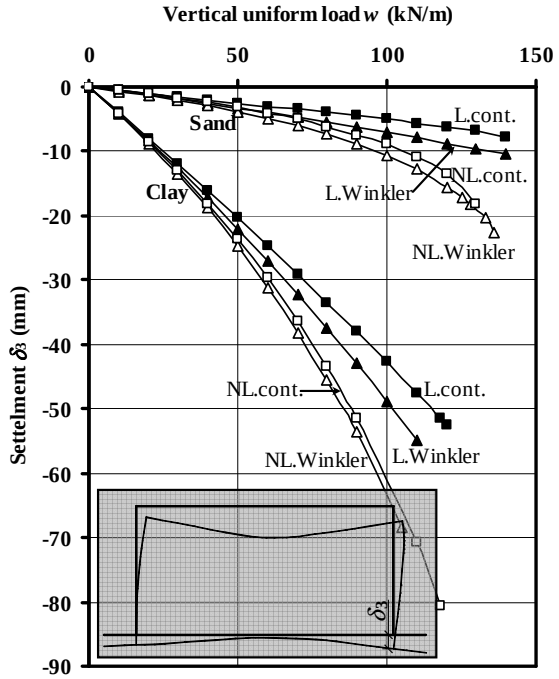

Fig. 28 Load versus settlement at bottom section of right column

On this basis, the resulting differential settlement and curvature of the strip footing are much more considerable for clay soils. Accordingly, the resulting bending moments in the footing supported by clay are greater.

From Figs. 27 and 28, it can be noticed that Winkler's settlement predictions at midspan of strip footing are smaller than those of the continuum model. The contrary is true at column base; as the Winkler's settlement predictions therein are bigger. Therefore, the resulting differential settlement, and hence the bending moments, in the footing are bigger for Winkler's model, if compared with continuum model.

One of the most interesting options available in NARC, is its capability to display and plot the distribution of residual flexural rigidity for the entire frame at any loading stage. Moreover, the corresponding distributions of strains and stresses for both concrete and rebar at any cross section can be also displayed, as shown in Figs. 29 and 30.

The Winkler's predictions for bending moments in the strip footing are bigger than the continuum model predictions, as stated earlier. Consequently, deterioration of flexural rigidities of footing sections in a specific region as predicted by Winkler's model happens earlier, if compared with continuum model. This can easily be noticed from Figs. 29 and 30 that illustrate the distribution of residual flexural rigidity for the entire frame as predicted by both models. Careful investigation of both figures shows that both distributions of residual rigidity along the frame members are almost identical. However, the loads causing the deterioration in both cases are quite different. For the distribution of residual flexural rigidity shown in Fig. 29, which was predicted via Winkler's model, the applied load was 70 kN/m. On the other hand, the results shown in Fig. 30, were achieved by the continuum model when the load reached 110 kN/m (about 57% higher than the load applied with Winkler's model).

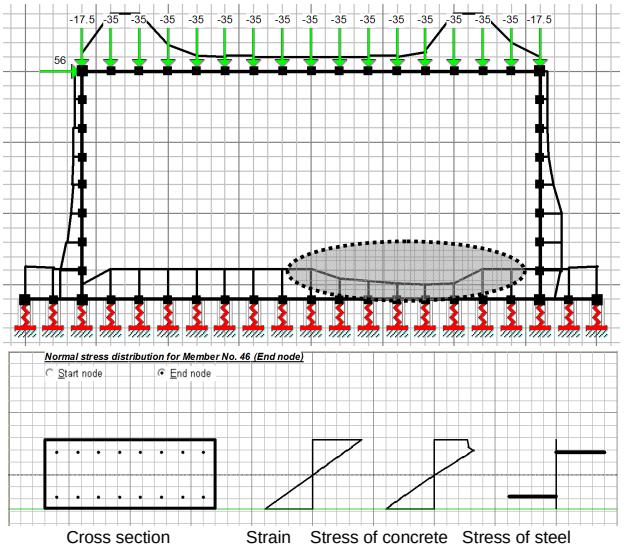

Fig. 29 Residual flexural rigidity at w = 70kN/m and normal stress distribution for foundation cracked section (L. Winkler)

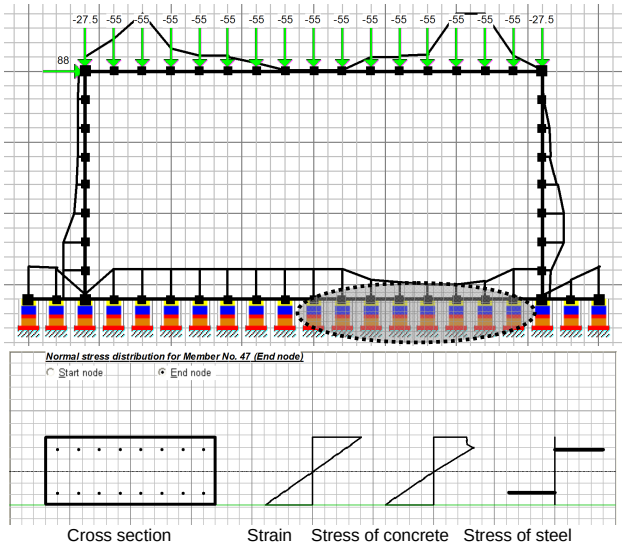

Fig. 30 Residual flexural rigidity at w = 110kN/m and normal stress distribution for foundation cracked section (L. cont.)

VI. Conclusions

A nonlinear finite element model, in the form of a computer program, was presented for the soil-structure interaction analysis of plane framed structures up to failure. The material and geometrical nonlinearities for both concrete and rebar are taken into account. 4-different models are available in the program to consider the soil behavior based on Winkler's and continuum formulations. The program is capable to list the full details of the soil-structure nonlinear analysis. It can also display and plot the frame deformations, soil settlement, internal forces, strain, and stress distributions along the RC cross sections, in addition to the distribution of axial as well as flexural residual rigidities for all members. The present analysis procedure and the program were validated by comparing the results with previous theoretical and experimental tests. An application of the proposed model on a rectangular RC frame subjected to vertical and lateral loads, with different soil conditions was also introduced for demonstration. Analysis results confirmed the expected structural behavior of the frame up to failure, which is governed by the details of RC sections, material properties, as well as the type of soil. The frame drift increases linearly with increasing loads up till cracking of RC sections, then the frame exhibits nonlinear strain hardening response up till the ultimate strength, which is encountered when the rebar fails.

References

[1] Dunder, C., (1990), "Concrete Box Sections Under Biaxial Bending and Axial Load", ASEC Journal, Vol. 116, No. 3, pp. 860-865.

[2] Kwat, H. G. and Filippou, F. C., (1997), "Nonlinear FE Analysis of R/C Structures Under Monotonic Loads", Computer & Structures Journal, Vol. 65, No. 1, pp. 1-16.

[3] Anam, I. and Shoma, Z. N., (1999), "Nonlinear Properties of Reinforced Concrete Structures", Internet report, http://www.uapbd.edu/cee/Bulletin /8.FAnamSir-22.pdf.

[4] Ibrahim, F. K. and Zubydan, A. H., (2002), "Geometric and Material Nonlinear Analysis of R. C. Frames", Ain Shams University, Faculty of Engineering, Scientific Bulletin, Cairo, Vol. 37, No. 3, pp. 61-74.

[5] Hassan, M. M., (2002), "Stability Analysis of Frames Considering Soil-Structure Interaction", Ms.c. Thesis, Department of Civil Engineering, Suez Canal University, Port Said, Egypt.
[6] Jahromi, H. Z., Izzuddin, B. A., and Zdravkovic, L., (2009), " A Domain Decomposition Approach for Coupled Modeling of Nonlinear Soil–Structure Interaction", Computer Methods in Applied Mechanics and Engineering, Vol. 198, Issues 33–36, pp. 2738-2749.
[7] Zubydan, A. H., (2000), "Simplified Model for R. C. Plane Frame Structures Considering Axial Effect", Ain Shams University, Faculty of Engineering, Scientific Bulletin, Cairo, Vol. 35, No. 3, pp. 15-27.
[8] Kandil, O. A., (2006), "Nonlinear Analysis of Reinforced Concrete Structures", Ms.c. Thesis, Department of Civil Engineering, Suez Canal University, Port Said, Egypt.
[9] Renata S.B. Stramandinoli, Henriette L. La Rovere, (2008),"An Efficient Tension-Stiffening Model for Nonlinear Analysis of Reinforced Concrete Members", Engineering structural Journal, Vol. 30, pp. 2069–2080.
[10] Chapra, S. C. and Canale, R. P. (2002), "Numerical Methods for Engineering", Fourth Edition, Mc Graw Hill, New York.
[11] Nassef, W. M., (2010), " Behavior of Structural Systems at Elevated Tempera-tures", Ms.c. Thesis, Department of Civil Engineering, Suez Canal University, Port Said, Egypt.
[12] Chen, W. F. and Lui, E. M., (2000), "Stability Design of Steel Frames", Boca Raton, Floreda.
[13] El-Gendy, M. M., (1999), "An Iterative Procedure for Foundation Superstructure interaction Problem", Port-Said Engineering Research Journal, Vol.3, No.I, pp. 1-19.
[14] Egyptian Code of Soil Mechanics and Design & Implementation of Foundation, (2001), No.202/3, Second Edition.
[15] Juvandes LFP., (1999), "Reforço e Reabilitação de Estruturas de Betão Usando Materiais Compósitos de “CFRP””, Ph.D. Thesis, University of Porto, Portugal.
[16] Vecchio, F. J. and Emara, M. B. (1992), "Shear Deformations in Reinforced Concrete Frames", ACI Structural Journal, Vol. 89-S6, No. 1, pp. 46-56.